Examination of source fault model for the Gifu-Ichinomiya fault based on seismic intensity data

Masayuki Kuriyama[1], Hiroaki Sato[1], and Tomotaka Iwata[2]

[1]*Central Research Institute of Electric Power Industry, Civil Engineering Research Laboratory, 1646, Abiko, Abiko-shi, Chiba 270-1194, Japan*
[2]*Disaster Prevention Research Institute, Kyoto University, Gokasho, Uji-shi, Kyoto 611-0011, Japan*

To investigate possible source fault models for the Gifu-Ichinomiya fault, we construct multiple source fault models of the 1891 Nobi earthquake, taking into account several different types of geometry for the Gifu-Ichinomiya fault, and conduct strong ground motion simulations. We choose the most plausible source model by comparing the distribution of simulated seismic intensities with the spatial distribution of a questionnaire-based intensity of 7, and with that of the damage ratio of wooden houses in the near-source region. Our results imply that the length of the source fault of the Gifu-Ichinomiya fault is relatively short and the dip angle is 75 degrees to the east. Because a seismic intensity of 7 is considered to arise from site amplification and the short distance from a source fault, we classified the points with a seismic intensity of 7 based on the H/V spectral ratio of microtremors by considering the contributing factors to the generation of a seismic intensity of 7. A linear distribution of the points, which might have relatively lower site amplification factors, in the northeastern part of the Nobi Plain implies that a part of the source fault of the 1891 Nobi earthquake existed in this area, as indicated through strong ground motion simulations.

Key words: The 1891 Nobi earthquake, Gifu-Ichinomiya fault, seismic intensity data, strong ground motion simulation, H/V spectral ratio of microtremors.

1. Introduction

Investigation of source fault models of multi-fault rupture events in long active fault zones is the key to understanding the characteristics of great inland crustal earthquakes and the behavior of rupture segments. The 1891 Nobi earthquake, which generated surface earthquake faulting along known active faults (such as the Nukumi fault, the Neodani fault and the Umehara fault, shown in Fig. 1), was one of the greatest inland crustal earthquakes ever recorded in Japan. Kuriyama and Iwata (2011) examined the construction methodology of a source model for strong ground motion prediction of a scenario earthquake for the Nobi earthquake. They conducted strong ground motion simulations using an empirical Green's function method (Hartzell, 1978; Irikura, 1986) based on assumed characterized source models (Irikura and Miyake, 2001). Through a comparison of the seismic intensities obtained from simulated waveforms and those estimated from questionnaire-based intensities determined by Muramatu and Kominami (1992) over a wide area, Kuriyama and Iwata (2011) determined the most plausible source-model construction methodology. Furthermore, their results suggested that the Gifu-Ichinomiya fault, which is buried beneath the Nobi Plain, might have ruptured during the 1891 Nobi earthquake. However, near the Gifu-Ichinomiya fault, Kuriyama and

Iwata (2011) compared the simulated and estimated seismic intensities at only a few stations. Therefore, they could not discuss its geometry in detail.

Meanwhile, a planar distribution map of the damage ratio of wooden houses was obtained near the source fault of the 1891 Nobi earthquake (Muramatu, 1983). By using seismic intensity data evaluated from both the questionnaire-based intensities and the damage ratio of wooden houses, it might be possible to examine the geometry of the Gifu-Ichinomiya fault in detail. In this study, we attempt to reproduce the distribution of a questionnaire-based intensity of 7 in the Nobi Plain, with strong ground motion simulations, by using a subsurface structure model for this area and several source fault models that take into account the geometry of the Gifu-Ichinomiya fault. We choose the most plausible source model by comparing the distribution of simulated seismic intensity for each model with the distribution of the questionnaire-based intensity (Muramatu and Kominami, 1992) and with the distribution of the damage ratio of wooden houses (Muramatu, 1983) in the near-source region. In order to improve the reliability of the source model, we discuss the reproducibility of the distribution of a questionnaire-based intensity of 7 for various source fault models: our models and models presented in previous researches.

Additionally, points having a questionnaire-based intensity of 7 had a planar distribution in the Nobi Plain (Fig. 1). Such a characteristic distribution might be caused by a rupture of the Gifu-Ichinomiya fault and the site amplification effect of sedimentary layers in the plain. Therefore, we
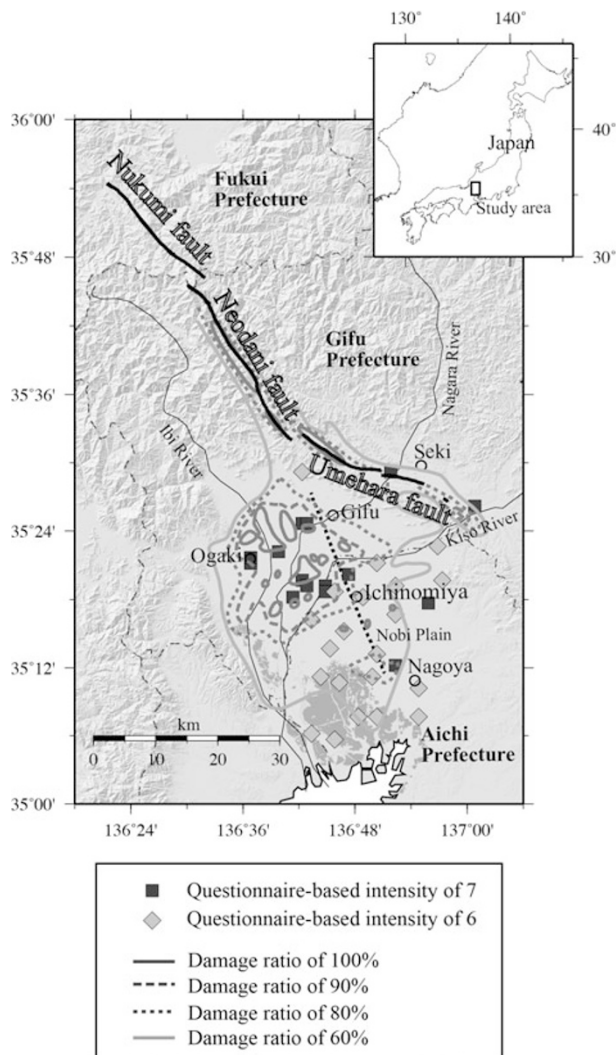
Fig. 1. Distribution of questionnaire-based intensity of 6 and 7 determined by Muramatu and Kominami (1992) and distribution of damage ratio of wooden houses based on Muramatu (1983). The thick black lines show the locations of surface earthquake faults of the 1891 Nobi earthquake. The broken black line indicates the location of the Gifu-Ichinomiya fault of the Research Group for Active Faults of Japan (1991). Chain lines show the locations of borders between prefectures. The shaded relief map is based on the dataset of 10-m DEM (Digital Elevation Model) of the Geospatial Information Authority of Japan (GSI).

also classified the points having a questionnaire-based intensity of 7 based on the predominant period of the ratio between the horizontal and vertical Fourier amplitudes of microtremors (Nakamura and Ueno, 1986) by taking into consideration the contributing factors of a questionnaire-based intensity of 7. Based on the distribution of the points having a re-evaluated intensity of 7, we discuss the length of the source model of the Gifu-Ichinomiya fault.

2. Distributions of Seismic Intensity Data near the Gifu-Ichinomiya Fault

The seismic intensity scale used in Japan is the scale of the Japan Meteorological Agency (hereafter, referred to as the JMA). This seismic intensity is measured from instrumentally-recorded ground motion data (JMA, 1996). Meanwhile, the seismic intensity scale of JMA from 1949 to 1996 had been determined from the damage situation of

structures and the other information (JMA, 1996). At that time, a seismic intensity scale having 8 degrees from 0 to 7 was applied. This seismic intensity scale of 7 corresponds to the destructive ground motion that causes the higher ratio of collapsed houses. Here, we assume that the JMA seismic intensity scale from 1949 to 1996 is equivalent to the scale from 1996.

To obtain dense seismic intensity distributions, questionnaire surveys have been conducted. In the case of the 1891 Nobi earthquake, the previous Tokyo Imperial University conducted a nationwide questionnaire survey about one month after the earthquake. Muramatu and Kominami (1992) determined a questionnaire-based intensity at each questionnaire survey point by relating these responses to the seismic intensity scales of JMA. They applied the seismic intensity scales of JMA which had been used from 1949 to 1996.

In the distribution of questionnaire-based intensities of 7, it is found that 1 questionnaire-survey point is located near the Umehara fault, and 13 survey points are located in the Nobi Plain (Fig. 1). Meanwhile, the questionnaire-survey points with a questionnaire-based intensity of 6 are mostly located in the southern part of the Nobi Plain. From the distribution in Fig. 1, it can be seen that questionnaire-based intensities are relatively higher in the northwestern part of the Nobi Plain.

Muramatu (1963, 1983) determined the damage ratios of wooden houses during the 1891 Nobi earthquake for each district in the Gifu Prefecture and the Aichi Prefecture. From Fig. 1, we can see that the areas with a damage ratio greater than, or equal to, 60% are distributed along the traces of the Neodani fault and the Umehara fault in the mountainous areas, and in the Nobi Plain. The area with a damage ratio greater than, or equal to, 80% in the northern part of the Nobi Plain extends along the Kiso River. This characteristic distribution might arise from site amplification. Areas with a damage ratio of 100% are sparsely located in the Gifu Prefecture. By comparing the distribution of the damage ratio in the Aichi Prefecture with that in the Gifu Prefecture, Muramatu (1983) interpreted that the cause of the distribution of damage ratios of 100% in the Gifu Prefecture could be ascribed to the short distances from the source fault and the site conditions.

From the relationship between the questionnaire-based intensity and the damage ratio, it is found that most questionnaire-survey points with a questionnaire-based intensity of 7 have a damage ratio greater than, or equal to, 80%. In this study, we assume that the questionnaire-based intensity at survey points with a damage ratio of greater than, or equal to, 80% is 7. Here, we also assume that the questionnaire-based intensity is equivalent to the JMA seismic intensity scale, as in the case of Kuriyama and Iwata (2011).

Miyakoshi *et al.* (2003) estimated the distribution of the peak ground velocity (hereafter, referred to as PGV) during the 1891 Nobi earthquake. This PGV distribution was obtained by using the relationships between the distributions of the damage ratios of wooden houses, the distributions of seismic intensity, and vulnerability functions between the PGV and damage ratios during the 1995 Hyogoken Nanbu

earthquake. However, Miyakoshi *et al.* (2003) also showed that the accuracy of the estimated PGV distribution was equal to that of the isoseismal distribution. In this study, to examine the most plausible source model, we apply seismic intensity data, which are evaluated from questionnaire-based intensities, and the damage ratio of wooden houses.

3.　Characteristics of the Gifu-Ichinomiya Fault

For the buried active fault in the Nobi Plain, Sugisaki and Shibata (1961) recognized that, based on existing boring data, the Ichinomiya-Inasawa fault might have displaced a pumice bed. By following subsurface geological data and leveling results before and after the 1891 Nobi earthquake, the Research Group for Active Faults of Japan (1991) also identified that the buried active fault (hereafter referred to as the Gifu-Ichinomiya fault) extends from the northwestern part of Gifu City to Nagoya City. The length of this buried fault is estimated to be 32 km. Meanwhile, based on the subsurface geological profiles and the results of *P*-wave seismic reflection surveys of the Aichi Prefecture (1998), it was suggested that the Gifu-Ichinomiya fault had not been ruptured repeatedly, although it could not be concluded that no active fault exists. From the profiles of *P*-wave seismic reflection surveys of the Aichi Prefecture (2000), it was found that no cumulative displacements, which are caused by faulting, could be observed near the Gifu-Ichinomiya fault. Later, Sugisaki and Shibata (2003) investigated, in detail, the existing boring data in the Nobi Plain. They described the Gifu-Ichinomiya fault as being located about 1.5 km east of the location identified by the Research Group for Active Faults of Japan (1991).

According to the Headquarters for Earthquake Research Promotion (2001), a possibility that the buried fault under the Nobi Plain was one of the source faults of the 1891 Nobi earthquake had first been inferred by Kizawa and Yamawa (1891) and by Katayama (1893) based on the distribution of the heavily damaged zone. Muramatu (1963) indicated that one of the source faults of the 1891 Nobi earthquake is located along the boundary between the uplift zone and the subsidence zone based on the distribution of seismic intensities and the distribution of coseismic vertical displacements.

Based on geodetic and seismologic methods, the following source models have been proposed for the Nobi earthquake. Mikumo and Ando (1976) calculated the theoretical vertical displacements on the basis of several fault plane models and compared them with the observed vertical displacements along two leveling routes across the Umehara fault and the buried fault. By applying the forward modeling method, they found that movements of four faults, including the buried fault, were needed to explain the observation. In their fault models, the buried fault has a dip of 90 degrees and extends from the southern part of the Neodani fault to Ichinomiya City, with a length of 34 km.

Fukuwa *et al.* (2003) calculated the peak horizontal velocities on the engineering bedrock, for their three assumed models of the 1891 Nobi earthquake, by applying the attenuation relation of Si and Midorikawa (1999), and calculated peak ground velocities using the amplification factor of Matsuoka and Midorikawa (1993). They obtained a

distribution of seismic intensities based on the relationship between the peak horizontal ground velocity and seismic intensity (Midorikawa *et al.*, 1999), and compared this with the distribution of the damage ratio of wooden houses (Muramatu, 1983). They found that the distribution of the calculated seismic intensities for their model, which was constructed by referring to the distribution of coseismic displacement and that of micro-earthquakes, corresponds to the distribution of the damage ratio rather than the distribution of calculated seismic intensities from the model of Mikumo and Ando (1976). For the Gifu-Ichinomiya fault, Fukuwa *et al.* (2003) assumed a reverse fault with an inclined fault plane having a length of 35 km and a dip of 70 degrees.

Nakano *et al.* (2007) applied the inversion method to the coseismic vertical displacements along two leveling routes across the Umehara fault and the buried fault in order to establish a fault model of the Gifu-Ichinomiya fault. They obtained a fault model having an inclined fault plane with a dip of 60 degrees located 5 km east of the location put forward by Mikumo and Ando (1976). As described above, various interpretations have been proposed for both the existence, and the geometry, of the Gifu-Ichinomiya fault. In this study, we examine the source fault model of the Gifu-Ichinomiya fault by attempting to reproduce the distribution of seismic intensity data in the Nobi Plain using strong ground motion simulations.

4.　Strong Ground Motion Simulations of the 1891 Nobi Earthquake

4.1　Construction of source fault models

With the aim of constructing a source fault model of the 1891 Nobi earthquake, the rupture of the Gifu-Ichinomiya fault during the earthquake, and its fault geometry, have been discussed (Mikumo and Ando, 1976; Fukuwa *et al.*, 2003). Here, we construct various source fault models that take into account several types of geometries for the Gifu-Ichinomiya fault (Gifu-Ichinomiya segment). Table 1 shows the length and the dip angle (east dipping) of the Gifu-Ichinomiya segment for each model. We also show

Table 1.　Length and dip angle (east dipping) of the Gifu-Ichinomiya segment for each model. In Model C, the Gifu-Ichinomiya segment is not included in the source fault model.

Model	Segment length(km)	Dip angle (degrees)
A-1		90
A-2	31.6[*1]	75
A-3		60
B-1		90
B-2	24.0[*2]	75
B-3		60
C	—	—
D[*3]	35.0	90
E[*4]	34.0	70

[*1] The Research Group for Active Faults of Japan (1991)

[*2] This study

[*3] Mikumo and Ando (1976)
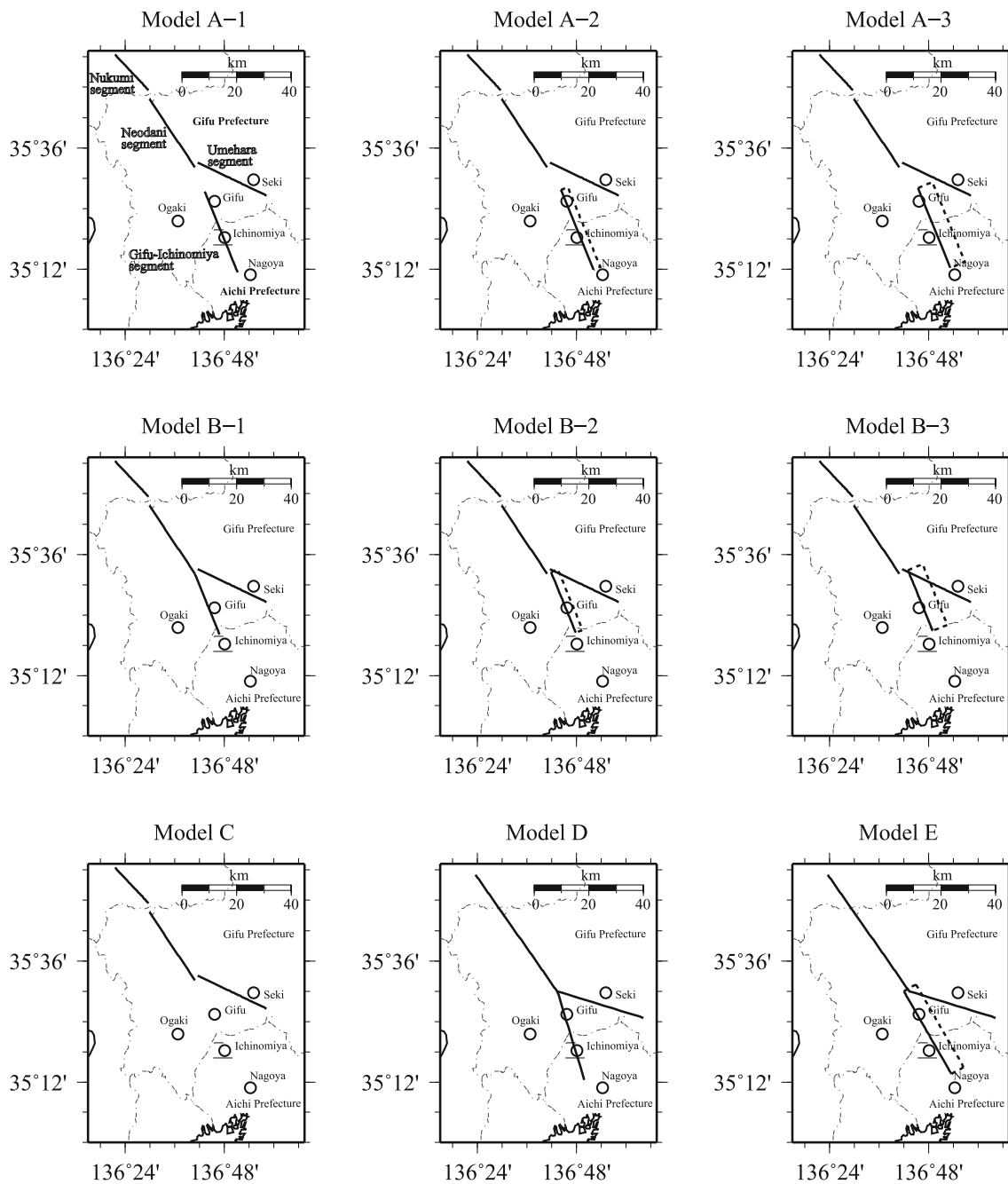
[*4] Fukuwa *et al.* (2003)

Fig. 2. Location of the Nukumi, Neodani, Umehara, and Gifu-Ichinomiya segments for each model (thick black lines). For the Gifu-Ichinomiya segment, the thick black line and broken lines indicate the location of the fault plane projected on the ground surface. The thick black lines show the location of the upper limit of the assumed fault plane. Two thin black lines indicate the locations of the seismic reflection surveys of the Aichi Prefecture (1998). Chain lines show the locations of borders between prefectures.

the location of the Nukumi, Neodani, Umehara, and Gifu-Ichinomiya segments for each model in Fig. 2.

Model A includes the entire Gifu-Ichinomiya fault suggested by the Research Group for Active Faults of Japan (1991). The location of this model is the same as that of the most plausible source model of Kuriyama and Iwata (2011). Although the Gifu-Ichinomiya fault of Model A might be located far from the other faults, it is possible that the rupture could propagate across the 10-km discontinuity, as in the case of the 1668 earthquake in the North Anatolian fault system reported by Kondo (2009). In this model, the length of the Gifu-Ichinomiya segment is approximately

32 km. However, the results of the *P*-wave seismic reflection surveys of the Aichi Prefecture (1998) could suggest the non-existence of the Gifu-Ichinomiya fault. In Model B, we assume that the Gifu-Ichinomiya segment extends from the southern end of the surface earthquake fault of the 1891 Nobi earthquake along the Neodani fault to the northern part of the Gifu-Ichinomiya fault, as recognized by the Research Group for Active Faults of Japan (1991), so as not to cross the lines of the seismic reflection surveys of the Aichi Prefecture (1998). In Model B, the length of the Gifu-Ichinomiya segment is assumed to be 24 km.

During the 1891 Nobi earthquake, an uplift zone and a

Table 2. Lengths and widths of each segment.

	Segment	Model A	Model B	Model C	Model D	Model E
Rupture length (km)	Nukumi	16.7			18.0	
	Neodani	29.8			34.0	
	Umehara	27.8			33.0	
Rupture width (km)	Nukumi	12.0				
	Neodani	15.0			15.0	
	Umehara	16.0				
	Gifu-Ichinomiya	10.0(A-1,B-1) 10.4(A-2, B-2) 11.5(A-3, B-3)			13.0	15.0

subsidence zone were generated along a boundary on the Nobi Plain extending from Gifu City to Nagoya City (e.g. Muramatu, 1963; Iseki, 1966). To take into account the distributions of the uplift zone and the subsidence zone, we also assume a reverse fault that has an inclined fault plane as the Gifu-Ichnomiya fault. Dip angles of the fault plane of the Gifu-Ichinomiya segment are then assumed to be 90 degrees (Model A-1, B-1), 75 degrees (Model A-2, B-2), and 60 degrees (Model A-3, B-3) by referring to the source models of previous studies (Nakano *et al.*, 2007). In this study, we adopt 6 km as the depth of the upper limit of the fault plane of the Gifu-Ichinomiya segment based on microseismic activity in this area. Here, the location where the upper limit of the fault plane reaches the ground surface is approximately consistent with the location of the boundary between the uplift zone and the subsidence zone. We qualitatively confirm that the pattern of the distribution of vertical displacements, which are calculated by using MICAP-G (Naito and Yoshikawa, 1999) for fault models including the Gifu-Ichinomiya fault with the inclined fault plane, could be mostly similar to the pattern of the distribution of the uplift zone and the subsidence zone (Iseki, 1966). In the calculations of the vertical displacements, we applied the heterogeneous slip distribution of the characterized source model, which is described later. We also assumed that the rake angles for the Nukumi, Neodani, and Umehara segments are 0 degrees. Meanwhile, the rake angle of the Gifu-Ichinomiya segment is assumed to be 45 degrees.

We also assume a source model (Model C) that does not include the Gifu-Ichinomiya fault in order to confirm that the distribution of seismic intensities of 7 could not be reproduced by that simulation. For these 7 models, the width of each segment is obtained from the lower cutoff depth of microseismic activity, the depth of the upper limit of the fault plane, and the dip angle assumed for each segment. For the northwestern part of the Nukumi fault (Nukumi segment), the Neodani fault (Neodani segment), and the Umehara fault (Umehara segment), we apply the same geometrical parameters as those used in Kuriyama and Iwata (2011).

We also apply two fault models (Model D and Model E) that refer to previous fault models (Mikumo and Ando, 1976; Fukuwa *et al.*, 2003). The dip angles of the Gifu-Ichinomiya segment in Models D and E are 90 degrees and 70 degrees, respectively. For the Nukumi segment, the Neodani segment and the Umehara segment, the dip angles are 90 degrees in all models. In Table 1 and Table 2, the length and the width of each segment are listed.

We use a characterized source model proposed by Irikura and Miyake (2001), which is one of the most reliable approaches for broadband strong ground motion prediction, as a source model for strong ground motion simulation. For constructing the characterized source model, we follow a procedure described in the Headquarters for Earthquake Research Promotion (2008) and in Irikura and Miyake (2010). We also refer to the characterized source models used in Kuriyama and Iwata (2011). Appendix A indicates the procedure in this research to construct characterized source models. Table 3 lists the fault parameters for each characterized source model. Figure 3 also shows the assumed characterized source models.

4.2 Synthesis of strong ground motions

A stochastic Green's function method (Kamae *et al.*, 1991) enables us to simulate strong ground motion based on the framework of the empirical Green's function method (e.g. Hartzell, 1978; Irikura, 1986), when there are no recorded waveforms of aftershocks, or of small earthquakes, in the near-source region. We simulate strong ground motions near the source region of the 1891 Nobi earthquake using the stochastic Green's function method. We estimate the most plausible fault model by comparing the distribution of simulated seismic intensity with the distribution of evaluated seismic intensity data. Figure 4 shows a flowchart of the procedure used to calculate the seismic intensity on the ground surface and to estimate the most plausible fault model.

We first calculate the stochastic Green's function of a virtual middle-size earthquake by using the spectral model that follows the ω^{-2} model and the envelope model. We sum the stochastic Green's functions of the virtual middle-size earthquake and simulate strong ground motion on the engineering bedrock for each constructed model at the calculation points.

The Fourier amplitude spectrum of acceleration on the bedrock is calculated by applying Eq. (1) based on Boore (1983),

$$|A(\omega)| = \frac{R_{\theta\phi} \cdot \text{FS} \cdot \text{PRITIN}}{4\pi\rho\beta^2} \cdot m_0 \cdot \frac{(2\pi f)^2}{1 + (f/f_c)^2}$$
$$\cdot \frac{1}{\sqrt{1 + (f/f_m)^{2s}}} \cdot \frac{e^{-\pi f X/Q\beta}}{X^n} \quad (1)$$

The variables and their values are listed in Table 4. The envelope model for the crustal earthquake of Ho and Kawase (2007) is applied.

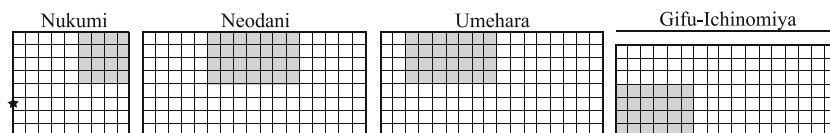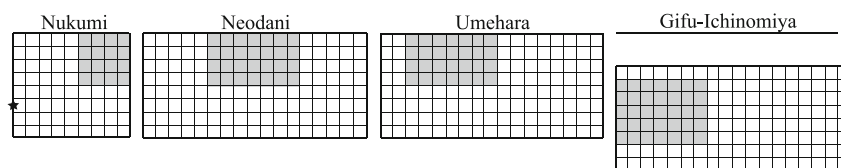(a) Model A, Model B, and Model C
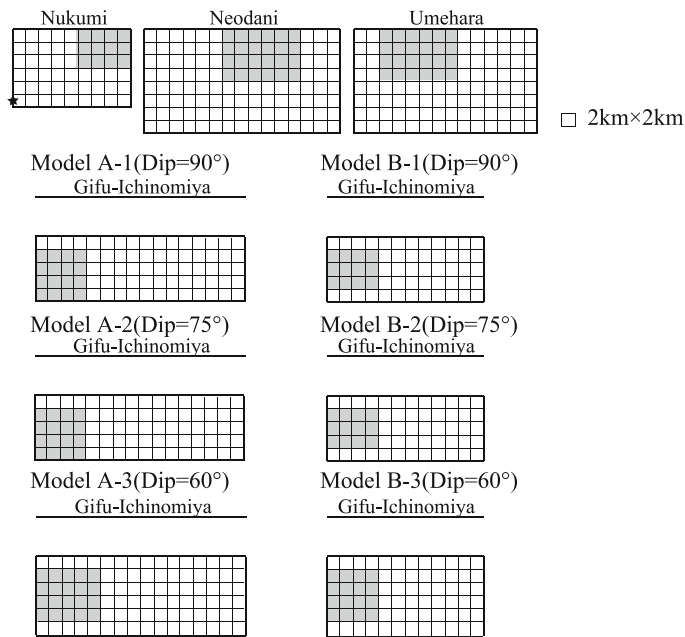
Fig. 3. Assumed characterized source models of the 1891 Nobi earthquake. Dark gray rectangles show the locations of asperities. Stars indicate the assumed rupture starting points.

Table 3. Source fault parameters for the assumed characterized source model.

Model	A-1	A-2	A-3	B-1	B-2	B-3
Total rupture length (km)	106			98		
Total rupture area (km^2)	1408	1419	1457	1332	1341	1369
Total seismic moment (N m) (Moment Magnitude)	1.10E+20 (7.3)	1.12E+20 (7.3)	1.18E+20 (7.3)	9.87E+19 (7.3)	1.00E+20 (7.3)	1.04E+20 (7.3)
Combined asperity area total rupture area (%)	22					
Stress drop on asperity MPa	23.1	23.2	23.5	22.5	22.6	22.8

Model	C	D	E
Total rupture length (km)	74	119	120
Total rupture area (km^2)	1092	1717	1800
Total seismic moment (N m) (Moment Magnitude)	6.64E+19 (7.2)	1.64E+20 (7.4)	1.80E+20 (7.4)
Combined asperity area total rupture area (%)	22		
Stress drop on asperity (MPa)	20.4	25.6	26.1

The acceleration waveforms of the virtual middle-size earthquake are calculated on the engineering bedrock with an *S*-wave velocity of greater than or equal to 600 m/s by applying the multiple reflection theory to the acceleration waveforms, which are simulated on the seismic bedrock. We assume the vertically incident *S* waves to the seismic bedrock. We utilize the subsurface structure model of the Chukyo area proposed by Horikawa *et al.* (2008) and apply

Table 4. List of the variables used for calculating Fourier amplitude spectra.

|	Variable	Value	Unit	Reference
$R_{\theta\phi}$	Radiation coefficient for an *S*-wave	0.63	—	Boore (1983)
FS	Amplification due to a free surface	1	—	Boore (1983)
PRITIN	Factor for partitioning energy into two horizontal components	0.707	—	Boore (1983)
ρ	Density below the bedrock	2.7	g/cm^3	
β	*S*-wave velocity below the bedrock	3.46	km/s	
m_0	Seismic moment for a virtual middle-size earthquake	—	N m	
f	Frequency	—	Hz	
f_c	Corner frequency	—	Hz	
f_m	Cutoff frequency	6.0	Hz	Satoh (2002)
s	Decay rate at high frequencies	2.1		Satoh *et al.* (1994)
X	Source distance	—	km	
Q	Path attenuation	$204\,f^{0.65}$	—	Kawase and Matsuo (2004)
n	Geometrical attenuation factor	$1.0(X<100)$ $0.95(100<X<120)$	—	Kawase and Matsuo (2004)
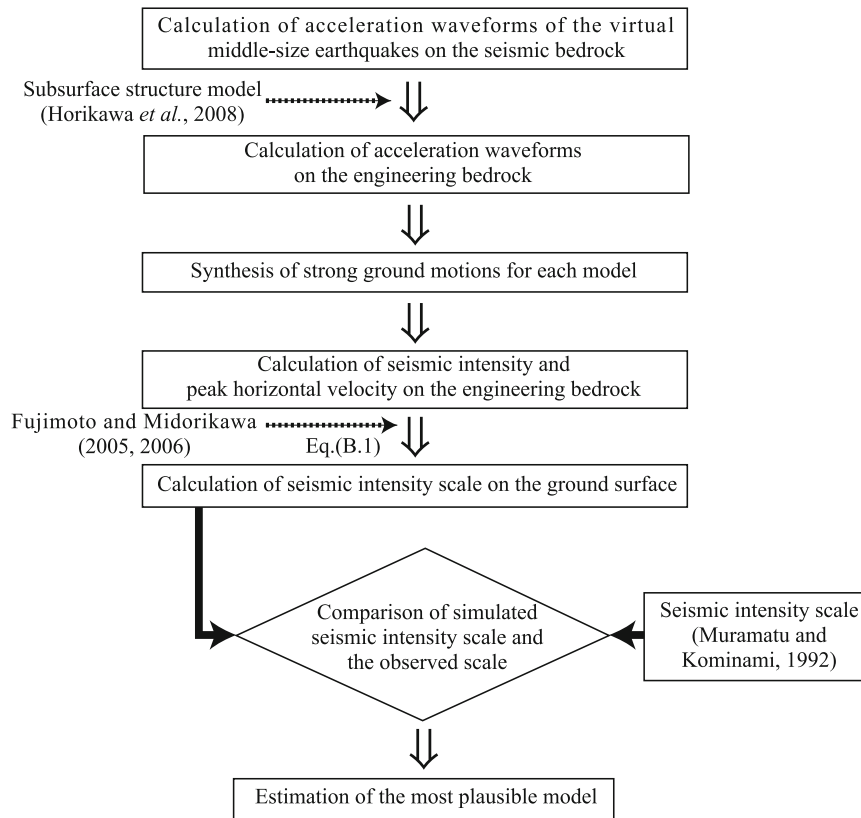
Fig. 4. Flowchart of the procedure to estimate the most plausible model.

the model from the upper surface of the seismic bedrock to the upper surface of engineering bedrocks. We also refer to the structural model of the *Q*-value at GIFH09 (Hashima) obtained by the Japan Atomic Power Company *et al.* (2010) and Umeda and Kobayashi (2010).

To sum up the simulated acceleration waveforms on the engineering bedrock for the virtual middle-size earthquake, we follow the framework of the empirical Green's function method (Irikura, 1986) between the seismic moment of a scenario earthquake and that of a virtual middle-size earthquake. For the virtual middle-size earthquake, we assume a source fault with a size 2 km by 2 km, and a seismic moment

obtained by using the source fault parameters of the background slip area for each characterized source model. Here, we also assume that the static stress drop for the virtual middle-size earthquake is the same as the effective stress of the background slip area for each model.

We synthesize strong ground motion waveforms on the engineering bedrock at each base mesh (approximately 1 km by 1 km) in the area from the northwestern end of the Nukumi fault to the southern part of the Nobi Plain. At each base mesh, we compute the seismic intensity on the engineering bedrock from synthesized strong ground motion waveforms by referring to a procedure of JMA (1996). For

calculating a seismic intensity on the ground surface, we apply the method shown in Appendix B. We use a random initial value for the phase spectrum to generate the stochastic Green's functions. We then conduct strong ground motion simulations 10 times by applying the different random values and obtain the average seismic intensity on the ground surface of those 10 simulations at each base mesh. The seismic intensity scale obtained here corresponds to that of JMA which has been used since 1996.

5. Comparison of the Distributions of Simulated Seismic Intensities with the Distribution of Evaluated Seismic Intensity Data

We choose the most plausible source model by referring to the number of points with a simulated seismic intensity scale equal to the questionnaire-based intensity of 6 or 7 among the 22 points in the areas extending from Ogaki City and Gifu City to Nagoya City. We also compare the distributions of simulated seismic intensity of 7 with the distribution of damage ratio greater than, or equal to, 80%. Figure 5 shows the number of points with a simulated seismic intensity scale equal to the questionnaire-based intensity for each source fault model. Figure 6 shows the distributions of the simulated seismic intensities for each model and the location of the 22 points used to evaluate the source fault models.

The number of points with a simulated seismic intensity scale equal to the questionnaire-based intensity of 6 or 7 is the highest in the case of Model B-2 (Fig. 5). Therefore, we can regard Model B-2 as the most plausible source model among the assumed models. According to the distribution of simulated seismic intensity for Model B-2 (Fig. 6), seismic intensities of 7 are distributed along the Nukumi segment, the Neodani segment, and the Umehara segment, and in the areas extending from the northwestern part to the southeastern part of the Nobi Plain. The distribution of a simulated seismic intensity of 7 for Model B-2 is approximately consistent with the planar distribution of damage ratios greater than, or equal to, 80% (Fig. 1), although the simulated seismic intensities may be slightly overestimated in the area extending from Ichinomiya City to Nagoya City and along the Kiso River.

For Model A-1, which includes the Gifu-Ichinomiya fault shown in the Research Group for Active Faults of Japan (1991), the simulated seismic intensity scales are overestimated at all questionnaire-survey points with the questionnaire-based intensity of 6. Although the damage ratios are less than 60%, which would be equivalent to a seismic intensity of less than 6, seismic intensity scales of 7 are simulated in the western areas of Nagoya City.

For Model C, which does not include the Gifu-Ichinomiya fault as the source fault of the 1891 Nobi earthquake, base meshes with a simulated seismic intensity of 7 are distributed mainly in the Gifu Prefecture and along the Kiso River (Fig. 6). However, a seismic intensity of 7 is not simulated in the area extending from Ogaki City to Ichinomiya City. Because the pattern of this distribution does not correspond to that of the distribution of damage ratios greater than, or equal to, 80%, the result of strong ground motion simulation for Model C is underestimated.
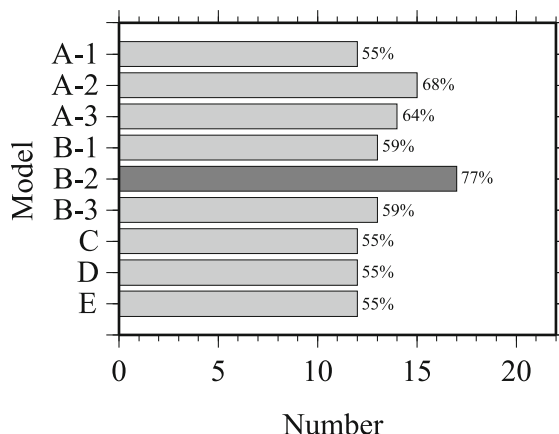

Fig. 5. Numbers of the points with a simulated seismic intensity scale equal to the seismic intensity scale of Muramatu and Kominami (1992) for each model. The total number of the points used to choose the most plausible source model is 22. The percentage is the ratio between the number of points with a simulated seismic intensity scale equal to the observed seismic intensity scale and the total number of points.

In the distributions for Models D and E, meshes with a seismic intensity of 7 are distributed along the Nukumi, Neodani, and Umehara segments (Fig. 6). For these models, meshes with a seismic intensity of 7 are also distributed throughout most of the Nobi Plain. Although the simulated seismic intensities in the area extending from Ogaki City to Ichinomiya City are equal to the observed seismic intensities (Muramatu and Kominami, 1992), the simulated seismic intensities in the area extending from Ichinomiya City to Nagoya City are overestimated. For the Nobi Plain, the area with overestimated intensities in these models, which is greater than the area with overestimated intensities in Model B-2, is considered to arise from the size of the fault plane of the Gifu-Ichinomiya fault and the static stress drop on the asperity.

From Fig. 5, it is also found that the number of points with a simulated seismic intensity scale equal to the questionnaire-based intensity is relatively higher in the source models that include the inclined fault plane with angles of 75 degrees for the Gifu-Ichinomiya segment (Models A-2 and B-2). Our results suggest that the inclined fault plane of the Gifu-Ichinomiya segment is needed to reproduce the distribution of observed seismic intensities in the Nobi Plain. It may also indicate that the length of the source fault of the Gifu-Ichinomiya fault is shorter than previously thought. In the following section, we discuss the length of the Gifu-Ichinomiya segment using an alternative approach.

6. Examination of the Location of the Source Fault Based on the Re-evaluated Seismic Intensity Data

The conditions required to generate a seismic intensity of 7 have been found to be related to the distance from the source fault and the ground conditions. For example, Midorikawa and Goso (1997) indicated that, for earthquakes with a magnitude of 8, the seismic intensity of 7 tends to be generated at alluvial sites, and that areas with such a seismic intensity extend up to 20 km from the source fault.
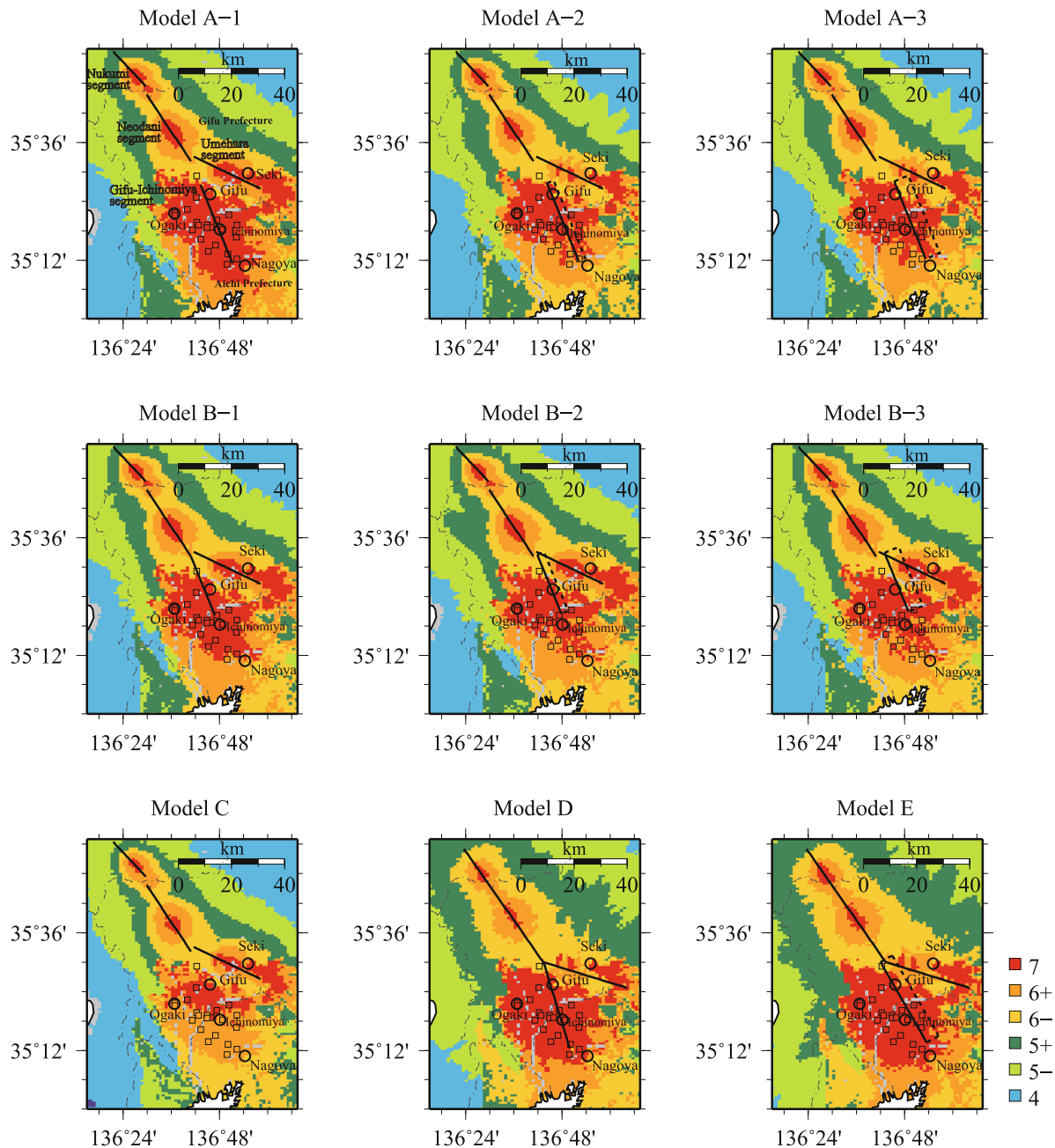
Fig. 6. Distributions of simulated seismic intensities for Models A–E. Solid lines and broken lines show the location of the Nukumi, Neodani, Umehara, and Gifu-Ichinomiya segments. Squares show the locations of the 22 questionnaire-survey points with a questionnaire-based intensity of 6 or 7. Chain lines show the locations of borders between prefectures.

Takemura *et al.* (1998) also demonstrated that, for inland earthquakes since the Meiji-Era, the causes responsible for generating a seismic intensity of 7 could be related to the distance from the source fault and to the site conditions. In the previous section, we proposed that the Gifu-Ichinomiya segment has an east-dipping fault plane and that its length may be shorter than previously thought. Here, we discuss the length of the Gifu-Ichinomiya segment based on the distribution of seismic intensity data re-evaluated by considering the conditions required to generate a seismic intensity of 7.

6.1 Classification of the points with a seismic intensity of 7 based on the predominant period of the H/V spectral ratio

Nakamura and Ueno (1986) proposed using the ratio between the horizontal and vertical Fourier amplitudes (hereafter referred to as the H/V spectral ratio) for approximating the transfer function of the ground at a given site. This method has been applied to examine easily the ground conditions. Kanno *et al.* (2008) indicated that the predominant period of the ground estimated from the spectral ratio of earthquake motions between the surface and a borehole, and the predominant period estimated by the H/V spectral ratio,
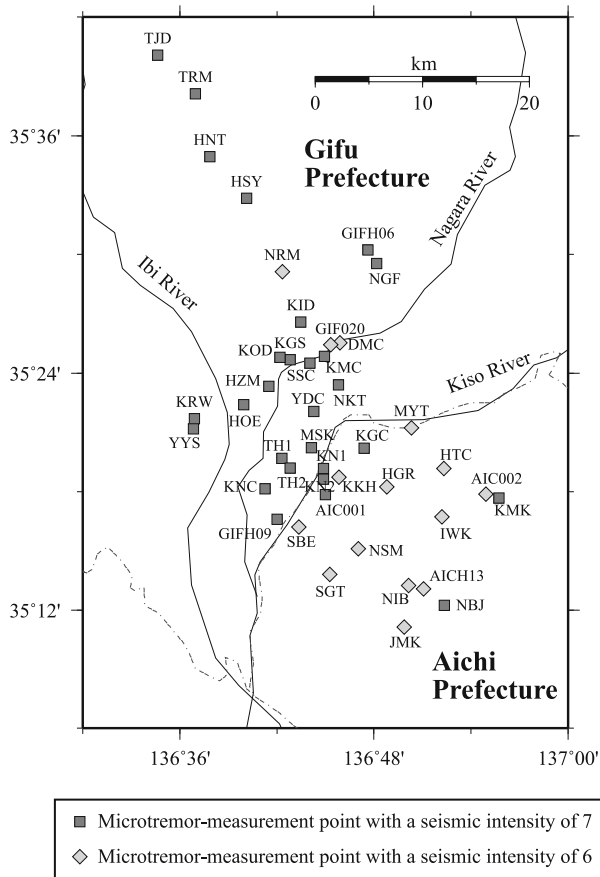
Fig. 7. Distribution of microtremor-measurement points. Seismic intensities at each point are estimated based on the questionnaire-based intensity of Muramatu and Kominami (1992) and the damage ratios of wooden houses of Muramatu (1983). As shown in the text, the seismic intensity might not be representative of Komaki City at KMK. Chain lines show the locations of borders between prefectures.
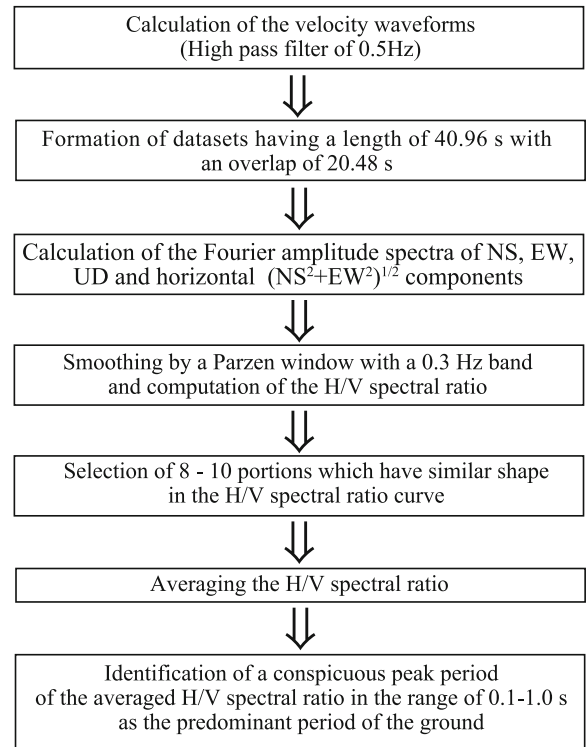

Fig. 8. The procedure used to obtain the predominant period of the H/V spectral ratio of the microtremors.
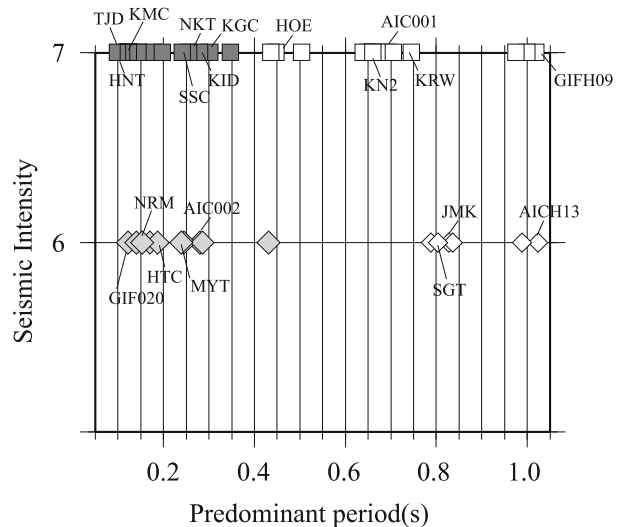

Fig. 9. Relationship between the predominant periods of the H/V spectral ratio of microtremors and the estimated seismic intensities based on the questionnaire-based intensity of Muramatu and Kominami (1992) and the damage ratios of wooden houses of Muramatu (1983). Diamonds and squares show the points with a seismic intensity of 6 and 7, respectively. Closed symbols also indicate the points that have a predominant period shorter than approximately 0.4 s.

had a high correlation. Because the predominant period of the ground depends on the ground condition at a given site, we examine the characteristics of the ground conditions based on the predominant period of the H/V spectral ratio of microtremors at 43 points (Fig. 7). The seismic intensity scales at these points are given based on the questionnaire-based intensity (Muramatu and Kominami, 1992) and the damage ratio (Muramatu, 1983). Anomalously, although the seismic intensity is 7 at KMK, the damage ratio is less than 50%. At KMK, the seismic intensity might not be representative of Komaki City.

For our measurements, we used a portable seismograph (GPL-6A3P) made by the Akashi Corporation (now the Mitsutoyo corporation); the seismograph comprises an overdamping acceleration sensor (V243FA), a data logger with a 24-bit A/D converter, an amplifier and filter component, and a battery. The measurable frequency range was 0.07–100 Hz. We chose an amplifier gain of 500 and measured the microtremors for about 10 minutes with a sampling rate of 100 Hz at each measurement point. Figure 8 shows the procedure to obtain the predominant period of the H/V spectral ratio of the microtremors.

Figure 9 shows the relationship between the seismic intensities and the predominant periods of the H/V spectral ratio at 43 microtremor-measurement points. In Fig. 10, we also indicate examples of the H/V spectral ratios of microtremors. As can be seen in Fig. 9, the predominant periods of most of the points with a seismic intensity of 7 are in the range of approximately 0.1–0.8 s. Meanwhile, the predominant periods of the points with a seismic intensity of 6 are shorter than approximately 0.4 s or longer than
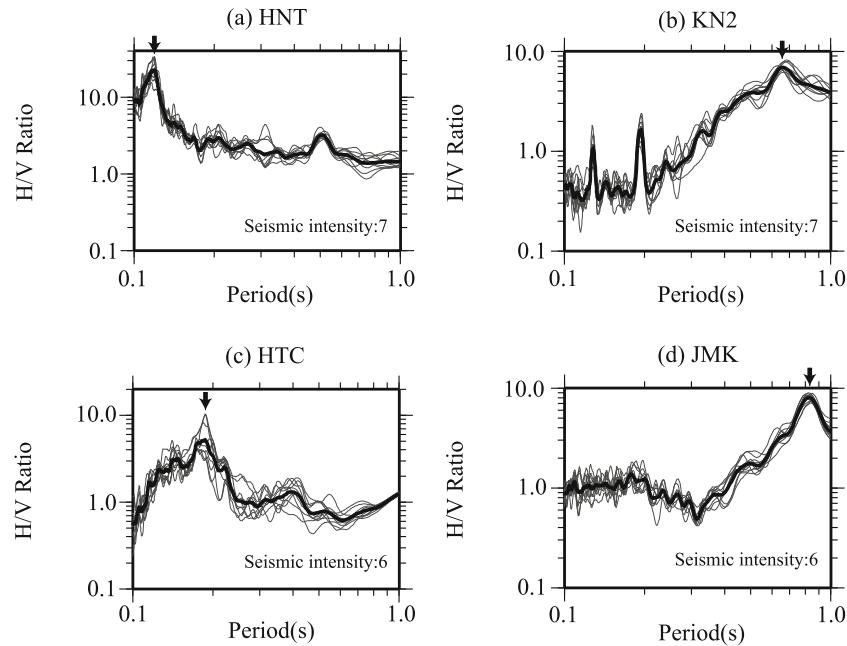
Fig. 10. Examples of H/V spectral ratios of microtremors. (a) HNT, (b) KN2, (c) HTC, and (d) JMK are representative of the points shown with closed squares, open squares, closed diamonds, and open diamonds in Fig. 9, respectively. At HNT with a predominant period shorter than 0.4 s, a seismic intensity of 7 can be primarily caused by the short distance from the source fault. At KN2 with a predominant period in the range of approximately 0.4–0.8 s, the generation of a seismic intensity of 7 can be a result of site amplification. The thin gray lines and thick black line indicate the H/V spectral ratios of selected portions of measured microtremors and their average, respectively. A solid arrow denotes the predominant period of the H/V spectral ratio.

approximately 0.8 s. Here, we suggest a method to classify the points with a seismic intensity of 7 based on the predominant period of the H/V spectral ratio. The ground conditions of the points with a predominant period in the range of approximately 0.4–0.8 s are considered to be soft ground, according to the classification of ground conditions (e.g. Molas and Yamazaki, 1995). Therefore, we consider that site-amplification factors at these points are relatively high. Based on this interpretation, the generation of a seismic intensity of 7 at points with a predominant period in the range of approximately 0.4–0.8 s (see Fig. 10(b)) can be a result of site amplification. Meanwhile, at points with a predominant period shorter than 0.4 s (see Fig. 10(a)), a seismic intensity of 7 can be caused primarily by the short distance from the source fault.

6.2 Discussion on the length of the Gifu-Ichinomiya segment based on the distribution of the points with a re-evaluated seismic intensity of 7

Figure 11 shows the distribution of points with a seismic intensity of 7. These points are classified into two groups in Subsection 6.1. It can be seen that four microtremor-measurement points near the Neodani fault and two near the Umehara fault have a predominant period shorter than 0.4 s (Fig. 11). As described above, the Neodani fault and the Umehara fault ruptured as the source fault in the 1891 Nobi earthquake. Although the site amplification factors at these points in the mountainous areas are relatively low, a seismic intensity of 7 might be generated because of the short distance from the source fault.

KGC, KID, KMC, NKT, and SSC in the northeastern part of the Nobi Plain have predominant periods shorter than approximately 0.3 s (Fig. 9). The site amplification factors at

these points are considered to be relatively lower than those in the western part of the plain (e.g. AIC001, HOE, KRW). Therefore, a seismic intensity of 7 might primarily arise from the short distance from the source fault at these points. As shown in Fig. 11, the linear distribution of these five points implies that the Gifu-Ichinomiya segment existed in the northeastern part of the Nobi Plain. This means that the length of the Gifu-Ichinomiya segment is shorter than that proposed in previous studies. The findings obtained here are also consistent with tectonic-geomorphological interpretations based on the results of *P*-wave seismic reflection surveys of the Aichi Prefecture (1998). Therefore, Model B, which includes the Gifu-Ichinomiya segment in the northeastern part of the Nobi Plain, is considered to be reliable.

7. Conclusions

We have examined the geometry of the Gifu-Ichinomiya fault, including the location, fault length, and dip angle, using seismic intensity data, which are evaluated from questionnaire-based intensities and the damage ratio of wooden houses, near the source region. For this purpose, we attempted to reproduce the distribution of the areas with a seismic intensity of 7 in the Nobi Plain by strong ground motion simulations based on characterized source models which take into account several types of geometries of the Gifu-Ichinomiya segment. We estimated the reverse fault with an east-dipping fault plane with a dip of 75 degrees as the source fault model of the Gifu-Ichinomiya segment. In this model, the Gifu-Ichinomiya segment has a length of 24 km, which is shorter than the length considered in previous models.

We also discussed the length of the Gifu-Ichinomiya seg-

- ■ Microtremor-measurement point with relatively lower site-amplification factor (Predominant period shorter than 0.4 s)
- □ Microtremor-measurement point with relatively larger site-amplification factor (Predominant period longer than 0.4 s)
- ⋯⋯ Gifu-Ichinomiya segment in Model A
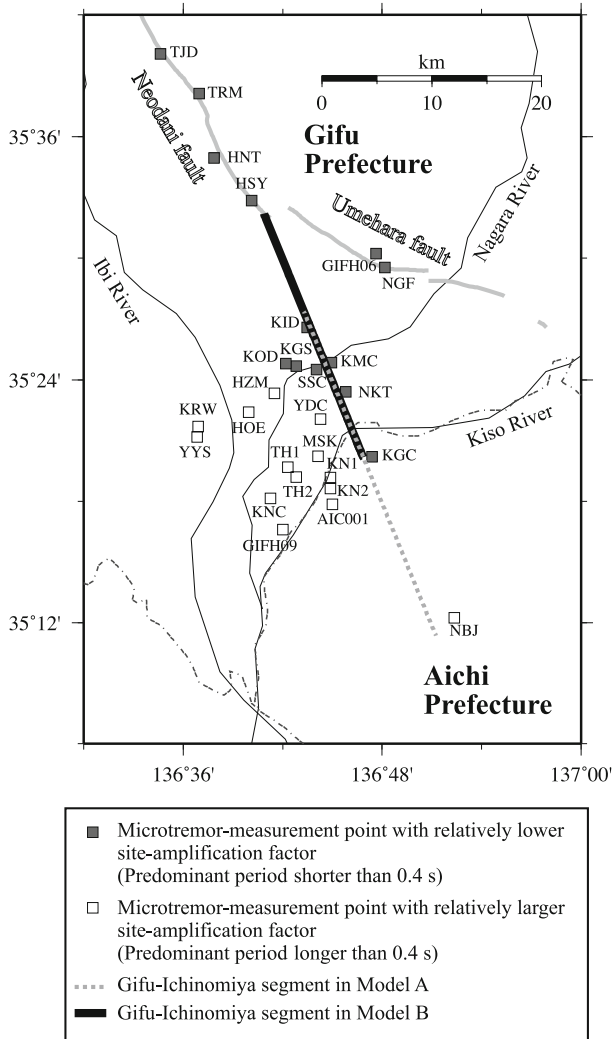- ▬▬ Gifu-Ichinomiya segment in Model B

Fig. 11. Distribution of classified microtremor-measurement points with a seismic intensity of 7. The thick gray lines show the locations of surface earthquake faults of the 1891 Nobi earthquake. Chain lines show the locations of borders between prefectures.

ment by suggesting an alternative approach. We classified the points with a seismic intensity of 7 based on the predominant period of the H/V spectral ratio of microtremors by considering the factors that contribute to the generation of a seismic intensity of 7. Because a seismic intensity of 7 can be caused primarily by a short distance from the source fault at the points having a predominant period shorter than 0.4 s, a linear distribution of these points in the northeastern part of the Nobi Plain implies that a part of the source fault of the 1891 Nobi earthquake existed in this area. This means that the length of the Gifu-Ichinomiya segment is shorter than the length proposed in previous studies. The findings obtained in this study are also consistent with tectonic-geomorphological interpretations based on the results of P-wave seismic reflection surveys of the Aichi Prefecture (1998). The method of examining the location of a source fault based on re-evaluated seismic intensity data is considered to be useful for estimating the geometry of the source faults of historical earthquakes.

Appendix A. A Procedure for Constructing Char-acterized Source Models in This Study

Here, we describe a procedure to construct characterized source models referring to a recipe (the Headquarters for Earthquake Research Promotion, 2008; Irikura and Miyake, 2010) for strong ground motion simulations. Figure A.1 shows the flowchart of the procedure used to characterize the fault parameters.

Kuriyama and Iwata (2011) state that the total seismic moment is constrained by the seismological scaling relationship for the 1891 Nobi earthquake. By referring to their results, we obtain the total seismic moment for each model from the total rupture area, by applying the empirical relationship given in Eq. (A.1):

$$M_0 = (S/4.24 \times 10^{11})^2 \times 10^{-7}, \qquad (A.1)$$

where M_0 is the seismic moment in N·m and S is the total rupture area in km^2. The total seismic moment is divided into the seismic moment for each segment by assuming that the stress drops are the same for each segment. We assume that the combined asperity area is about 22% of the total rupture area (Somerville et al., 1999). The stress drop on asperity is calculated by applying Eq. (A.2) to the equivalent radius of the combined asperity area and that of the source fault area.

$$\Delta\sigma_a = (7/16) \cdot M_0 \cdot (r^2 \cdot R). \qquad (A.2)$$

In Eq. (A.2), $\Delta\sigma_a$ is the static stress drop on asperity in MPa, r is the equivalent radius of the asperity in km, and R is the equivalent radius of the source fault in km. For the Nukumi segment, the Neodani segment, and the Umehara segment, we assume that the asperities are located where larger dislocations are observed on the ground by referring to the distribution of left-lateral displacements (Matsuda, 1974). For the Gifu-Ichinomiya segment, along which a surface earthquake fault did not appear during the 1891 Nobi earthquake, we assume the location of asperities by referring to the distribution of a high damage ratio of wooden houses (Muramatu, 1983). We chose the rupture starting point with a depth of 11 km at the northwestern end of the Nukumi segment by referring to Kuriyama and Iwata (2011).

A shear wave velocity of 3.46 km/s in the source region is used. We assume that the rupture propagates radially with an average velocity that is 72% of the shear wave velocity on the basis of Geller (1976). Except for the segment at which the rupture starts, segments rupture from the point that is the nearest to the edge of an already-ruptured contiguous segment. Different rupture starting times for different segments are obtained by considering the rupture propagation in the segment faults and the propagation of a shear wave in the gap between the segment faults.
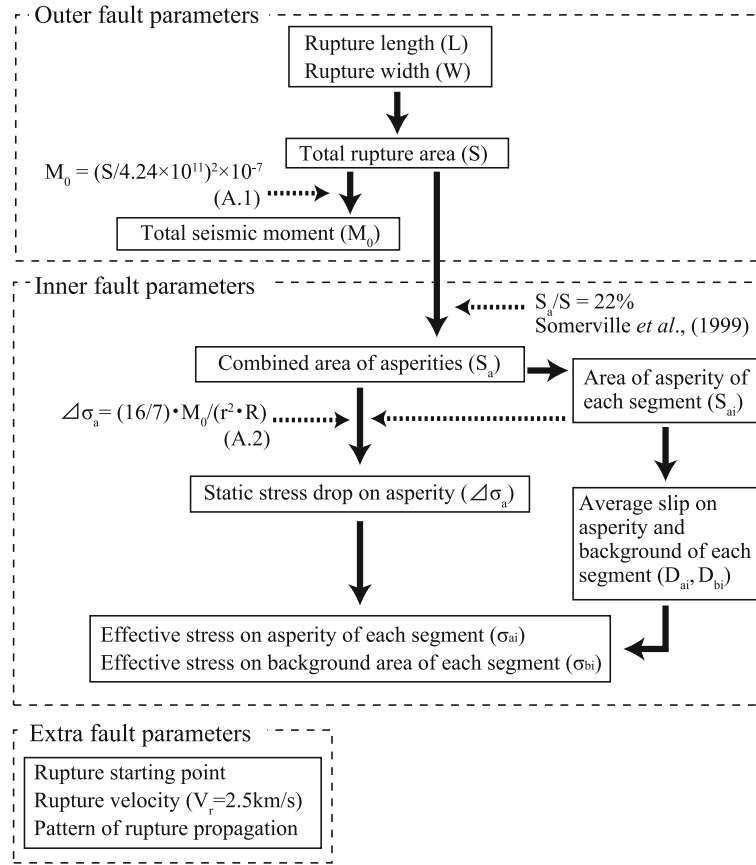
Fig. A.1. Flowchart of the procedure used to characterize fault parameters.

Appendix B. A Method for Calculating the Seismic Intensity on the Ground Surface

Here, we describe the method used to calculate a seismic intensity on the ground surface. A seismic intensity on the ground surface is calculated by applying Eq. (B.1), which is obtained from the relationship between seismic intensity and peak ground velocity (Fujimoto and Midorikawa, 2005) and the relationship between the average S-wave velocity of the ground and the amplification factor for soil with an S-wave velocity of 600 m/s (Fujimoto and Midorikawa, 2006):

$$I = 2.603 \cdot \log(\text{amp}) - 0.213 \cdot \log(\text{amp})^2$$
$$-0.426 \cdot \log(\text{PGV}_b) \cdot \log(\text{amp}) + I_b \quad \text{(B.1)}$$

In Eq. (B.1), I and I_b denote the seismic intensity on the ground surface and that on the engineering bedrock with an S-wave velocity of 600 m/s, respectively. amp is the amplification factor for soil with an S-wave velocity of 600 m/s. PGV_b is the peak velocity on the engineering bedrock with an S-wave velocity of 600 m/s. Here, we used the average shear-wave velocity in the upper 30 m (Vs30) obtained by Matsuoka *et al.* (2005).

When the engineering bedrock at each calculation point has an S-wave velocity of greater than 600 m/s, we calculate the seismic intensity on the ground surface by applying Eqs. (B.2) and (B.3):

$$I = 2.603 \cdot \log(A \cdot \text{amp}_t) - 0.213 \cdot \log(A \cdot \text{amp}_t)^2$$

$$-0.426 \cdot \log(\text{PGV}_t) \cdot \log(A \cdot \text{amp}_t) + I_b, \quad \text{(B.2)}$$

$$A = (\text{amp}_{600}/\text{amp}_t), \quad \text{(B.3)}$$

where PGV_t and amp_t denote the peak velocity on the engineering bedrock with an S-wave velocity greater than 600 m/s and the amplification factor for soil with an S-wave velocity greater than 600 m/s.

References

Aichi Prefecture, *Research Report of the Gifu-Ichinomiya and Yoro-Kuwana-Yokkaichi Fault Zones*, 118 pp, 1998 (in Japanese).

Aichi Prefecture, Underground structure in the Nobi plain, 61-70, 2000 (in Japanese).

Boore, D. M., Stochastic simulation of high-frequency ground motions based on seismological models of the radiated spectra, *Bull. Seismol. Soc. Am.*, **73**, 1865–1894, 1983.

Fujimoto, K. and S. Midorikawa, Empirical method for estimating J.M.A. instrumental seismic intensity from ground motion parameters using strong motion records during recent major earthquakes, *J. Inst. Social Safety Sci.*, **7**, 214–246, 2005 (in Japanese with English abstract).

Fujimoto, K. and S. Midorikawa, Relationship between average shear-wave velocity and site amplification inferred from strong motion records at nearby station pairs, *J. JAEE*, **6**(1), 11–22, 2006 (in Japanese with English abstract).

Fukuwa, N., K. Yamaoka, M. Nakano, J. Tobita, T. Sato, and Y. Suzuki, Investigation for the mechanism of the seismic damage band on Nobi earthquake, *Report of Grants-in-Aid for Scientific Research* (Research Project Number F12480110), 2003 (in Japanese).

Geller, R. J., Scaling relations for earthquake source parameters and magnitudes, *Bull. Seismol. Soc. Am.*, **66**, 1501–1523, 1976.

Hartzell, S. H., Earthquake aftershocks as Green's function, *Geophys, Res. Lett.*, **5**, 1–4, 1978.

Ho, N. and H. Kawase, Broadband stochastic Green's functions based on observed data by strong motion networks and its application to Nankai earthquake, *J. Jpn. Assoc. Earthq. Eng.*, **7**, No.2, 2007 (in Japanese with English abstract).

Horikawa, H., M. Yoshimi, H. Sekiguchi, K. Yoshida, Y. Sugiyama, K Satake, N. Fukuwa, H. Suzuki, H. Matsuyama, L. Ying, and F. Takizawa, A three-dimensional subsurface structure model of the Chukyo area, central Japan, *Ann. Rep. Active Fault Paleoearthq. Res.*, **8**, 203–254, 2008 (in Japanese with English abstract).

Irikura, K., Prediction of strong acceleration motions using empirical Green's function, *Proc. 7th Japan Earthq. Eng*, 151–156, 1986.

Irikura, K. and H. Miyake, Prediction of strong ground motions for scenario earthquakes, *J. Geogr.*, **110**(6), 849–875, 2001 (in Japanese with English abstract).

Irikura, K. and H. Miyake, Recipe for predicting strong ground motion from crustal earthquake scenarios, *Pure Appl. Geophys.*, doi:10.1007/s00024-010-0150-9, 2010.

Iseki, H., The active fault in the Nobi Plain during the 1891 Nobi earthquake, *The Journal of the Faculty of Letters, Nagoya University*, **16**, 231–243, 1966 (in Japanese).

Japan Meteorological Agency, *Seismic Intensity*, Gyousei, Tokyo, 238 pp, 1996 (in Japanese).

Kamae, K., K. Irikura, and Y. Fukuchi, Prediction of strong ground motion based on scaling law of earthquake, *J. Struct. Constr. Eng., AIJ.*, **430**, 1–9, 1991 (in Japanese with English abstract).

Kanno, T., K. Miura, and C. Kumagai, Accuracy verification of estimation method for predominant period of ground at earthquake observation points in Chugoku district, *Geophys. Explor.*, **61**(6), 533–543, 2008 (in Japanese with English abstract).

Katayama, I., *Nobi Shinshi*, 241pp, 1893 (in Japanese).

Kawase, H. and H. Matsuo, Separation of source, path, and site effects based on the observed data by K-NET, KiK-net, JMA strong motion network, *J. Jpn. Assoc. Earthq. Eng.*, **4**, 1, 2004 (in Japanese with English abstract).

Kizawa, N. and Y. Yamawa, *Meiji Shinsai Shuroku*, 174 pp, 1891.

Kondo, H., Recurrence behavior and past multi-segment earthquakes on the North Anatolian fault system, *The Earth Monthly*, **31**(4), 231–242, 2009 (in Japanese).

Kuriyama, M. and T. Iwata, Examination of source-model construction methodology for strong ground motion simulation of multi-segment rupture during 1891 Nobi earthquake, *Earth Planets Space*, **63**, 71–88, 2011.

Matsuda, T., Surface faults associated with Nobi (Mino-Owari) earthquake of 1891, Japan, *Spec. Rep. Earthq. Res. Inst.*, **13**, 85–126, 1974 (In Japanese).

Matsuoka, M. and S. Midorikawa, Prediction of isoseismal map for large area using the digital national land information, *J. Struct. Constr. Eng., AIJ.*, **447**, 51–56, 1993 (in Japanese with English abstract).

Matsuoka, M., K. Wakamatsu, K. Fujimoto, and S. Midorikawa, Average shear-wave velocity mapping using Japan Engineering Geomorphologic Classification Map, *J. JSCE*, **794/I-72**, 239–251, 2005 (in Japanese with English abstract).

Midorikawa, S. and T. Goso, A study on occurrence rate of destructive ground motion based on case histories, *J. Struct. Constr. Eng., AIJ.*, **502**, 55–60, 1997 (in Japanese with English abstract).

Midorikawa, S., K. Fujimoto, and I. Muramatu, Correlation of new J.M.A. instrumental seismic intensity with former J.M.A. seismic intensity and ground motion parameters, *J. Social Safety Sci.*, **1**, 51–56, 1999 (in Japanese with English abstract).

Mikumo, T. and M. Ando, A search into the faulting mechanism of the 1891 great Nobi earthquake, *J. Phys. Earth.*, **24**, 63–87, 1976.

Miyakoshi, J., T. Sato, and N. Fukuwa, Distribution of ground motion intensity evaluated using wooden house damage during the 1891 Nobi earthquake (M8) in central Japan, *J. Inst. Social Safety Sci.*, **5**, 77–86, 2003 (in Japanese with English abstract).

Molas, G. L. and F. Yamazaki, Attenuation of earthquake ground motion in Japan including deep focus events, *Bull. Seismol. Soc. Am.*, **85**, 1343–1358, 1995.

Muramatu, I., Distribution of seismic intensity and crustal deformation in the region destroyed by the great Nobi earthquake of October 28, 1891, *Res. Rep., Gifu Univ.*, **3**, 202–224, 1963 (in Japanese).

Muramatu, I., Distribution of the percentage of collapsed houses in the Nobi plain for the Nobi earthquake of 1891, *Res. Rep., Gifu Univ.*, **7**, 867–882, 1983 (in Japanese with English abstract).

Muramatu, I. and M. Kominami, Collection of answers for a questionnaire investigation soon after the Nobi earthquake of 1891, *Technical Note of the National Research Institute for Earth Science and Disaster Prevention*, **155**, 1–841, 1992 (in Japanese with English abstract).

Naito, H. and S. Yoshikawa, A program to assist crustal deformation analysis, *Zisin, second series*, **52**, 101–103, 1999 (in Japanese).

Nakamura, Y. and M. Ueno, A simple estimation method of dynamic characteristics of subsoil, *Proc. 7th Japan Earthq. Eng.*, 265–270, 1986 (in Japanese with English abstract).

Nakano, M., J. Miyakoshi, and K. Yamaoka, A new model for the fault beneath the sedimentary basin in the 1891 Nobi earthquake, *Earth Planets Space*, **59**, 13–19, 2007.

Satoh, T., Radiation pattern and fmax of the Tottori-ken Seibu earthquake and the aftershocks inferred from KiK-net strong motion records, *J. Struct. Constr. Eng., AIJ.*, **556**, 25–34, 2002 (in Japanese with English abstract).

Satoh, T., H. Kawase, and T. Sato, Statistical spectral characteristics for engineering bedrock waves in which local site effects of surface geology are removed—Based on the ground motion records of small and medium earthquakes observed in the boreholes in Sendai—, *J. Struct. Constr. Eng., AIJ.*, **462**, 79–89, 1994 (in Japanese with English abstract).

Si, H. and S. Midorikawa, New attenuation relationships for peak ground acceleration and velocity considering effects of fault type and site condition, *J. Struct. Constr. Eng., AIJ.*, **523**, 63–70, 1999 (in Japanese with English abstract).

Somerville, P. G., K. Irikura, R. Graves, S. Sawada, D. Wald, N. Abrahamson, Y. Iwasaki, T. Kagawa, N. Smith, and A. Kowada, Characterizing crustal earthquake slip models for the prediction of strong ground motion, *Seismol. Res. Lett.*, **70**, 59–80, 1999.

Sugisaki, R. and K. Shibata, Geochemical study on ground water (I): subsurface geology and aquifers in the Nobi plain, *J. Geol. Soc. Jpn.*, **67**, 335–345, 1961 (in Japanese with English abstract).

Sugisaki, R. and K. Shibata, Reappraisal of the Gifu-Ichinomiya Fault— Points at issue for recognition of concealed fault under an alluvial plain, *Zisin, second series*, **56**, 281–296, 2003 (in Japanese with English abstract).

Takemura, M., T. Moroi, and K. Yashiro, Characteristics of strong ground motions as deduced from spatial distributions of damages due to the destructive inland earthquakes from 1891 to 1995 in Japan, *Zisin, second series*, **50**, 485–505, 1998 (in Japanese with English abstract).

The Headquarters of Earthquake Research Promotion, Evaluation of Gifu-Ichinomiya fault zone, http:// www.jishin.go.jp/main/chousa/ 01jan2/index.htm, 2001 (in Japanese).

The Headquarters for Earthquake Research Promotion, Strong ground motion prediction method ("Recipe") for earthquakes with specified source faults, http://www.jishin.go.jp/main/kyoshindo/08apr_kego/ recipe.pdf, 2008 (in Japanese).

The Japan Atomic Power Company, the Japan Atomic Energy Agency, and the Kansai Electric Power Company, Re-evaluation of the subsurface structure model to apply into the ground motion evaluation in Wakasa area, the 23th Joint Working Group for Earthquake, Tsunami, Geology, and Foundations under the Seismic and Structural Design Subcommittee, http://www.nisa.meti.go.jp/shingikai/107/3/ 4/023/23-2.pdf, 2010 (in Japanese).

The Research Group for Active Faults of Japan, *Active Faults in Japan*, 437 pp, University of Tokyo Press, 1991 (in Japanese).

Umeda, N. and K. Kobayashi, Study on estimation of deep underground structures by inversion of seismic records, *Proc. 13th Japan Earthq. En*, 2363–2369, 2010 (in Japanese with English abstract).

Wessel, P. and W. H. F. Smith, New, improved version of the Generic Mapping Tools released, *Eos Trans. AGU*, **79**, 579, 1998.

M. Kuriyama (e-mail: kuriyama@criepi.denken.or.jp), H. Sato, and T. Iwata